

RESEARCH ARTICLE

Adaptive Sliding Mode Control of an Electro-Hydraulic Actuator With a Kalman Extended State Observer

LIMING LAO^{ID} AND PENGZHAN CHEN^{ID}

Institute of Robotics and Intelligent Systems, Taizhou University, Taizhou, Zhejiang 318000, China

Corresponding author: Pengzhan Chen (cyxcpz@163.com)

This work was supported in part by the Scientific Research Project of the Education Department of Zhejiang Province under Grant Y202045664, in part by the Taizhou Science and Technology Plan Project under Grant 2002gy09, and in part by the Taizhou University Research Project under Grant 2019PY041.

ABSTRACT Electro-hydraulic actuators (EHAs) are key linear drive components in various industrial applications. This paper addresses the challenge of achieving precise displacement tracking control for EHAs with only noisy displacement measurements. We propose a novel control approach, which consists of a Kalman extended state observer (KESO) with an adaptive sliding mode controller (ASMC). First, compared to the conventional high-gain design for the extended state observer (ESO), the Kalman filtering technique is utilized to tune the ESO feedback gain, effectively mitigating observation failures caused by measurement noise. Second, to ensure stability and minimize tracking errors in sliding mode control, a switching-gain adaptation is designed based on the desired switching gain via the derivative of the sliding variable. To validate the effectiveness of the proposed approach, simulation experiments are conducted in the Amesim simulation software. The results conclusively demonstrate that the proposed KESO-ASMC achieves significantly improved trajectory tracking performance, even in the presence of measurement noise and unknown disturbances.

INDEX TERMS Adaptive switching gain, disturbance estimation, electro-hydraulic actuator, Kalman extended state observer, measurement noise, sliding mode control.

I. INTRODUCTION

The electro-hydraulic actuator (EHA) plays a crucial role as the primary driving mechanism in various heavy-duty applications, converting electrical energy into mechanical motion through the use of hydraulic fluid. These applications include industrial injection molding machines [1], shield tunneling machines [2], and aerospace rocket thrusters [3]. One fundamental control application of EHAs is the precise regulation of linear displacement in mechanical systems. However, EHAs are nonlinear systems with changing parameters and complex dynamics, including pressure fluctuations,

internal leakage, friction, and external loads dependent on operating conditions [4]. These characteristics pose challenges for achieving precise control over EHA displacement.

To address the parameter nonlinearities of EHAs, one approach is to employ a real-time parameter estimation method based on parameter projection [5], [6], [7]. Alternatively, nominal parameter values can be assigned, treating parameter variations as disturbances [4], [8], [9], [10]. Nonlinearities in the model can also be considered as disturbances to the nominal system. To counteract these disturbances, techniques like robust control [11], [12] and adaptive control [13] use feedback-based approaches. Observer-based control methods compensate for disturbances through disturbance observers [14], [15], [16], [17]. Sliding

The associate editor coordinating the review of this manuscript and approving it for publication was Jorge Esteban Rodas Benítez^{ID}.

mode control (SMC) is widely used in EHAs due to its conceptual simplicity and robustness against disturbances. By incorporating disturbance feedforward compensation, SMC reduces the switching actions required for stability in the presence of uncertainties.

Implementing SMC in hydraulic systems presents two primary challenges. Firstly, SMC requires the measurement of all system states, which can be challenging in practice. If the system model satisfies the Davidson-Kimura condition, static output feedback SMC can be applied [18]; otherwise, an observer or a dynamic compensator is needed. Secondly, designing an appropriate switching gain for disturbance suppression is crucial. Small switching actions can cause the system to deviate from the sliding surface, especially under significant uncertainties, leading to degraded system performance and potential instability. Conversely, large switching actions can excite high-frequency unmodeled system dynamics, resulting in chattering.

Various effective disturbance estimation techniques have been developed alongside SMC to mitigate uncertainties. The nonlinear disturbance observer (NDO) [17], [19] employs auxiliary variables to estimate disturbances when state derivatives are unknown, applied in the control of velocity and pressure dynamics [20]. The Sliding mode observers (SMO) achieves precise disturbance estimation through switching actions, addressing nonlinearity in pump control system dynamics [7], [21]. Recently, neural network based approaches have successfully achieved universal approximation of uncertain dynamics and disturbances [22], [23], [24], [25], [26]. Although these methods do not require knowledge of uncertainty bounds, they are complicated to implement and lack a systematic discussion concerning their training efficiency and over-fitting issues. The extended state observer (ESO) [27] is another simple yet effective method widely used for synchronized system state and disturbance estimation through nonlinear feedback. The linear ESO (LESO) [28], [29] replaces nonlinear feedback with linear high-gain feedback to suppress disturbances. ESO finds broad applications with sliding mode controllers in various mechanical and electronic systems, including power converters [30], [31], robotic manipulators [32], [33], drones [34], [35], and hydraulic systems [36], [37], [38], [39], for state observation and disturbance estimation.

However, limited work has thoroughly discussed the impact of measurement noise on ESO performance. A simple way to address this issue is by adding a low-pass filter prior to the ESO, but this method may compromise dynamic performance [40]. Another approach is to modify the ESO to make it suitable for a noisy environment. Simulation results from [41] and [42] indicate that significant noise is observed in tracking errors when the measured signal contains Gaussian white noise. Nevertheless, there has been little discussion regarding the effect of noise on ESO observations and parameter tuning. It has been suggested that increasing ESO bandwidth through high-gain feedback

can enhance estimation performance, but measurement noise constrains the available bandwidth [43], [44]. It's also argued that the accuracy of nonlinear ESOs depends on high gains, which can amplify noise and degrade control performance. To address this, the fal function in ESO has been replaced with the tanh function, which exhibits lower gains when estimation errors are small [39]. Another approach to mitigate the adverse effects of high gains on noise amplification is to adopt a cascade structure within the ESO [31]. Additionally, reduced-order ESO designs have been proposed to avoid noise amplification associated with high gains [45]. Departing from conventional strategies of nonlinear gain adaptation or reduced-order ESOs to address the impact of measurement noise, this paper introduces a novel approach: utilizing Kalman filter techniques to design ESO gains, resulting in the Kalman extended state observer (KESO).

Adaptive sliding mode control (ASMC) utilizes switching-gain adaptation to respond appropriately to system states and disturbances. Conservative adaptive laws [46], [47] dictate that the derivative of the switching gain is proportional to the sliding variable or error magnitude, resulting in a continuous increase of the switching gain until the sliding variable or error approaches zero. However, the main limitation is that the switching gain cannot decrease when the disturbance decreases, potentially causing chattering. Improved gain adaptation methods share a similar concept: they increase the gain when the sliding variable is small and decrease it when the sliding variable or error is large [48], [49], [50], [51], [52]. These methods differ in their boundaries for increasing and decreasing the switching gain, as well as the rates of increase and decrease. For instance, the adaptive law proposed by Tian et al. [48] swiftly replaces the switching gain with a predetermined maximum value when the sliding variable surpasses the boundary and decreases it within the boundary layer using a tracking differentiator. Li et al. [49] dynamically increased the switching gain until the sliding variable reaches a specified boundary and decrease it as the mean value of the switching action decreases. Tran et al. [50] adjusted the switching gain by increasing or decreasing it as the state control variables move away from or approach the sliding surface. Nevertheless, all these gain adaptation methods may fail to promptly increase the gain when dealing with a small sliding variable but a large disturbance because they all respond to the magnitude of the sliding variable or error.

This paper presents a conceptually simple and easy-to-implement KESO-ASMC scheme to address the displacement tracking control problem in practical EHAs with noisy displacement measurements. The KESO is designed to estimate unmeasurable system states and the lumped disturbance in the presence of measurement noise. An adaptive switching-gain sliding mode controller with disturbance feedforward compensation is responsible for tracking control. The main contributions of this paper can be summarized as follows:

- 1) We employ Kalman filtering technology to adjust the observer gain for the high-order LESO. Compared to the conventional high-gain tuning method of LESO, the proposed KESO effectively balances estimation accuracy with measurement noise attenuation, achieving satisfactory estimation performance even in the presence of significant measurement noise.
- 2) Inspired by pre-step disturbance estimation in discrete-time sliding mode, this paper introduces a novel switching-gain adaptation law based on the desired switching gain. This law has a clear design concept and responds quickly to sudden changes in disturbance, effectively balancing the requirements of robustness with chattering-free operation of SMC.

The remainder of this paper is organized as follows. Section II introduces the dynamic model of the electro-hydraulic actuator and outlines the problem formulation. Section III conducts the design of the Kalman extended state observer (KESO) and the adaptive sliding mode controller (ASMC) based on the desired switching gain. The simulation verification results are presented in Section IV. Finally, Section V provides the conclusion of this paper.

II. DYNAMIC MODEL OF THE EHA

In this paper, we introduce a variable speed pump controlled closed-circuit hydraulic actuator as an example of an EHA. The structure of the EHA, as depicted in Fig. 1, mainly consists of an electrical servo motor, a bidirectional fixed-displacement pump, and a double-rod hydraulic cylinder. An auxiliary oil source and a flushing valve are employed to maintain stable pressure in the low-pressure chamber and dissipate heat. To prevent overpressure, two relief valves are arranged in opposite directions. The moving part has a mass m_p and is subjected to an external load force F_L . The displacement of the piston rod, which corresponds to the load displacement, is denoted as x_p .

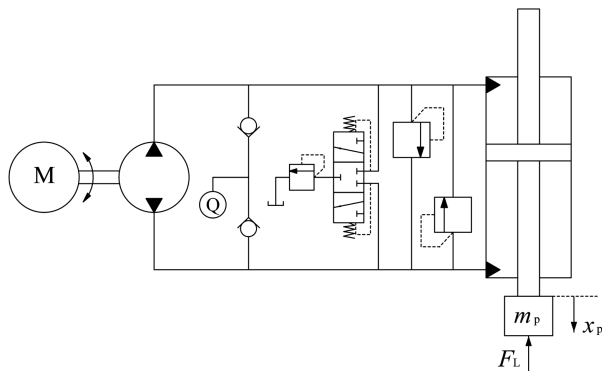


FIGURE 1. Schematic diagram of the electro-hydraulic actuator.

The high and low-pressure chambers of the EHA are influenced by the external load force, resulting in the load pressure exerting an opposing force. The pressure in the low-pressure chamber remains nearly constant, implying that its

pressure dynamics can be disregarded. Pressure dynamics caused by the pipelines are treated as disturbances, while external leakage is neglected. The four-quadrant operation of the EHA is determined by the directions of the load forces and the rotational orientations of the pumps. It can be derived that regardless of the operating quadrant, the EHA's load pressure dynamics can be characterized as [21]

$$\frac{V_c}{\beta_e} \frac{dp_L}{dt} + C_l p_L + A_p \frac{dx_p}{dt} + f_p = D_p \omega, \quad (1)$$

where p_L is the load pressure, V_c is the high pressure chamber volume which varies with piston displacement, β_e is the fluid's effective bulk modulus, A_p is the piston area, D_p is the displacement of the bidirectional pump, C_l is the total leakage coefficient, f_p is the unmodelled pipe dynamics, and ω is the rotational speed of the pump. The pump's speed is identical to that of the electrical servo motor, which is controlled by a high-performance vector control strategy integrated into the servo driver. The speed dynamics of the electrical motor operate at a significantly higher frequency band than the electro-hydraulic system. Therefore, the speed control model of the electrical motor can be regarded as

$$\omega = K_a u, \quad (2)$$

where u is the control input, K_a is the control gain.

The load dynamics follow Newton's third law and can be described as

$$m \frac{d^2 x_p}{dt^2} = A_p p_L - F_L - f_t, \quad (3)$$

where f_t is the total frictional force, which includes Coulomb friction and viscous friction. By deriving expressions for p_L and \dot{p}_L from (3), and substituting them into (1), we obtain the standard single-input single-output dynamics of the EHA, represented as

$$x_p^{(3)} = a_1 \dot{x}_p + a_2 \ddot{x}_p + bu + F, \quad (4)$$

with parameters $a_1 = -\frac{A_p^2 \beta_e}{m V_c}$, $a_2 = -\frac{C_l \beta_e}{V_c}$, $b = \frac{\beta_e A_p D_p K_a}{m V_c}$, and $F = -\frac{\dot{F}_L + \dot{f}_t}{m} - \frac{\beta_e (C_l F_L + C_l f_t + A_p \dot{f}_p)}{m V_c}$. Furthermore, defining the state vector as $X = [x_1 \ x_2 \ x_3]^T = [x_p \ \dot{x}_p \ \ddot{x}_p]^T$, the dynamic system is rewritten as

$$\begin{aligned} \dot{X} &= AX + B(u + b^{-1}F) \\ &= \begin{bmatrix} 0 & 1 & 0 \\ 0 & 0 & 1 \\ 0 & a_1 & a_2 \end{bmatrix} \begin{bmatrix} x_1 \\ x_2 \\ x_3 \end{bmatrix} + \begin{bmatrix} 0 \\ 0 \\ b \end{bmatrix} (u + b^{-1}F). \end{aligned} \quad (5)$$

Considering parameter variations, let A_n and B_n represent the nominal values of A and B , while ΔA and ΔB represent the parameter perturbations. Consequently, (5) can be further rewritten as

$$\begin{aligned} \dot{X} &= (A_n + \Delta A)X + (B_n + \Delta B)(u + b^{-1}F) \\ &= A_n X + B_n(u + d). \end{aligned} \quad (6)$$

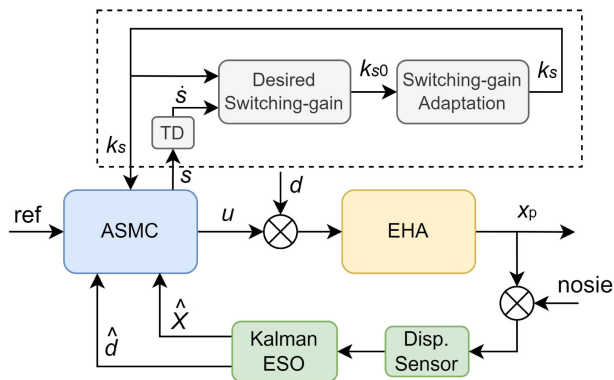


FIGURE 2. Block diagram of the proposed ASMC-KESO.

Here, d represents the lumped disturbance that encompasses unknown external loads, unmodeled dynamics, and parameter uncertainties, satisfying

$$B_n d = \Delta A X + \Delta B u + B b^{-1} F. \quad (7)$$

As only the displacement of the piston rod is measurable, the output equation can be denoted as

$$y = C X = [1 \ 0 \ 0] X. \quad (8)$$

III. ADAPTIVE SLIDING MODE CONTROL WITH KALMAN EXTENDED STATE OBSERVER

To achieve precise displacement tracking control for the EHA, it is essential to estimate both the system state variables and the lumped disturbance from the noisy displacement measurement signal. Additionally, the sliding mode switching gain needs adaptive adjustment to handle variations in unknown disturbances while maintaining stability and minimizing chattering. Fig. 2 illustrates the proposed controller structure, featuring a sliding mode controller with adaptive switching gain and a Kalman extended state observer.

A. KALMAN EXTENDED STATE OBSERVER

The unknown lumped disturbance can be incorporated into the extended system as an additional state variable, followed by the design of an observer for the observable extended system [16]. In the case of the EHA, only x_1 is directly measurable using the displacement sensor. However, due to factors like on-site electromagnetic noise, vibration of the hydraulic cylinder piston rod, and sensor measurement accuracy, x_1 comprises both the true value and measurement noise. The Kalman filter can estimate the unknown states in a dynamic system from noisy measurements using statistical information about random noise. This study employs the Kalman filtering technique to adjust the feedback gain of the extended state observer, facilitating the estimation of displacement, velocity, acceleration, and the lumped disturbance from the noisy displacement measurement signal.

Assuming that the lumped disturbance in the EHA exhibits relatively slow variations compared to the controlled system,

the differential of the disturbance can be modeled as zero-mean random white noise. Treating the disturbance as an additional state, the extended system is represented as [27]

$$\begin{cases} \begin{bmatrix} \dot{X} \\ \dot{d} \end{bmatrix} = \begin{bmatrix} A & B \\ 0 & 0 \end{bmatrix} \begin{bmatrix} X \\ d \end{bmatrix} + \begin{bmatrix} B \\ 0 \end{bmatrix} u + \begin{bmatrix} 0 \\ 1 \end{bmatrix} w \\ y = \begin{bmatrix} C & 0 \end{bmatrix} \begin{bmatrix} X \\ d \end{bmatrix} + v \end{cases} \triangleq \begin{cases} \dot{\bar{X}} = \bar{A} \bar{X} + \bar{B} u + F w \\ y = \bar{C} \bar{X} + v \end{cases}, \quad (9)$$

where \bar{X} is the extended state vector, \bar{A} , \bar{B} and \bar{C} are matrices appropriate for the extended system. v and w denote zero-mean white noise with variances R and Q , respectively. The KESO, which is a suboptimal steady-state Kalman filter, is designed for the extended system (9) as [53]

$$\begin{cases} \dot{\hat{X}}(t) = \bar{A} \hat{X}(t) + \bar{B} u + K [y(t) - \bar{C} \hat{X}(t)] \\ K = P \bar{C}^T R^{-1} \\ \bar{A} P + P \bar{A}^T + F Q F^T - P \bar{C}^T R^{-1} \bar{C} P = 0 \end{cases}, \quad (10)$$

where \hat{X} represents the estimation of \bar{X} and K is the steady-state Kalman gain. It can be easily verified that the matrix pair $[\bar{A}, F]$ is completely controllable, and the matrix pair $[\bar{A}, \bar{C}]$ is completely observable. Under those conditions, the stability of the Kalman filter type ESO is guaranteed [54]. The Kalman gain calculated by (10) depends on the variances of the process noise w and measurement noise v . Obtaining these variances in practical systems can be challenging. However, Theorem 1 demonstrates that this gain can be easily tuned.

Theorem 1: The Kalman gain K in (10) is determined solely by the ratio of the process noise variance Q to the measurement noise variance R , irrespective of the absolute values of Q and R .

Proof: Let K_0 be the Kalman gain when the noise variances are Q_0 and R_0 , satisfying the Riccati equation

$$\bar{A} P_0 + P_0 \bar{A}^T - P_0 \bar{C}^T R_0^{-1} \bar{C} P_0 + F Q_0 F^T = 0. \quad (11)$$

By multiplying both sides by a scaling factor β , we obtain

$$\begin{aligned} \bar{A} (\beta P_0) + (\beta P_0) \bar{A}^T + F (\beta Q_0) F^T \\ - (\beta P_0) \bar{C}^T (\beta R_0)^{-1} \bar{C} (\beta P_0) = 0. \end{aligned} \quad (12)$$

This implies that $P = \beta P_0$ is the solution to the Riccati equation when $Q = \beta Q_0$ and $R = \beta R_0$. Subsequently, the new Kalman gain is derived as

$$K' = (\beta P_0) \bar{C}^T (\beta R_0)^{-1} = P_0 \bar{C}^T R_0^{-1} = K_0. \quad (13)$$

Thus, we can conclude that the Kalman gain remains constant when the ratio of noise variances Q to R remains the same. \square

Remark 1: Theorem 1 demonstrates that the steady-state Kalman filter gain is solely determined by the ratio of variances between the process noise w and the measurement noise v , without consideration of their absolute values. As a result, we can adjust the Kalman feedback gain

by maintaining constant measurement noise variance and iteratively modifying the process noise variance. This trial-and-error method allows us to achieve the desired observer gain.

B. ADAPTIVE SWITCHING-GAIN SLIDING MODE CONTROL

1) SLIDING MODE CONTROL WITH OBSERVATIONS

The control objective is to ensure that the displacement of the piston rod x_1 of the EHA accurately follows the desired reference displacement x_d . The tracking error is denoted as $e = x_1 - x_d$. Furthermore, the reference vector is denoted as $X_d = [x_d \ \dot{x}_d \ \ddot{x}_d]$, and the error vector is $E = X - X_d = [e_1 \ \dot{e}_1 \ \ddot{e}_1]$. The linear sliding variable is defined as

$$s = S_c E. \tag{14}$$

Here, $S_c = [\lambda^2 \ 2\lambda \ 1]$, and the positive parameter λ regulates the speed of error convergence on the sliding surface. Considering state estimation, a sliding mode controller with switching action and disturbance compensation is designed as

$$u = (S_c B)^{-1} \left[S_c \dot{X}_d - S_c A \hat{X} - k_s \text{sgn}(\hat{s}) \right] - \hat{d}, \tag{15}$$

where $\text{sgn}(\bullet)$ represents the signum function. The switching-gain must satisfy the robust condition

$$k_s > |S_c A \tilde{X} + S_c B \tilde{d}|, \tag{16}$$

where $\tilde{X} = \hat{X} - X$ and $\tilde{d} = \hat{d} - d$ represent the state and disturbance estimation errors, respectively.

Remark 2: Due to the presence of state estimation error, $\text{sgn}(\hat{s}) = \text{sgn}(s + S_c \tilde{X})$. Therefore, $\text{sgn}(\hat{s}) = \text{sgn}(s)$ holds true only when $|s| = |S_c E| > |S_c \tilde{X}|$. Thus, sliding mode control based on state observers inherently results in a boundary layer with a thickness determined by the upper bound of $|S_c \tilde{X}|$.

2) ADAPTIVE SWITCHING-GAIN

Equation (16) necessitates that the value of k_s surpasses the upper bound of uncertainty. Opting for an excessively large k_s value leads to a conservative fixed gain and induces chattering. Conversely, selecting an overly small k_s value results in unstable sliding mode control. To introduce an adaptive law for the switching gain, it is imperative for the switching gain to automatically increase as uncertainty grows, as well as decrease.

By substituting the sliding mode control law (15) into the sliding variable (14), we can derive

$$\dot{s} = -S_c A \tilde{X} - S_c B \tilde{d} - k_s \text{sgn}(\hat{s}). \tag{17}$$

Thus, the uncertainty can be expressed as

$$|S_c A \tilde{X} + S_c B \tilde{d}| = |\dot{s} + k_s \text{sgn}(\hat{s})|. \tag{18}$$

The desired switching gain k_{s0} is defined as

$$k_{s0} = \left| \dot{s} + k_s \text{sgn}(\hat{s}) \right| + k_b > |S_c A \tilde{X} + S_c B \tilde{d}|, \tag{19}$$

where the derivative of the sliding variable \dot{s} is determined using methods such as tracking differentiators [55]. k_b represents the base switching gain employed to suppress uncertainties arising from sliding variable estimation and derivative errors.

Remark 3: The desired switching gain provides an estimation for the majority of varying uncertainties within the system. Compared with the conventional design of switching gain, this method only needs a smaller base gain k_b to suppress the remaining uncertainties, and can adapt according to the varying unknown disturbance. This concept of the desired switching gain is inspired by the common practice in discrete-time sliding mode control, which employs the previously computed disturbance value as an estimate for the current time step's disturbance [56]. This means that the uncertainty under the current switching control directly influences the changing rate of the sliding variable over time, and the inversely calculated value provides a good estimation of the uncertainty.

The explicit solution for the desired switching gain (19) cannot be obtained under the current sliding mode control due to the presence of the algebraic loop. Hence, the adaptive law for the switching gain is defined as

$$\dot{k}_s = \begin{cases} -\lambda_{ks} + \lambda_{ac} (k_{s0} - k_s), & k_s > k_{s0} \\ \lambda_{ks} + \lambda_{ac} (k_{s0} - k_s + |\hat{s}|), & k_s < k_{s0} \\ 0, & k_s = k_{s0} \end{cases}, \tag{20}$$

where λ_{ks} and λ_{ac} are positive parameters that satisfy $\lambda_{ks} > |\dot{k}_{s0} + \lambda_{ac} |S_c \tilde{X}|$.

3) STABILITY ANALYSIS

Theorem 2: According to the proposed sliding mode control law (15) and adaptive switching gain (20), the system is capable of converging towards the vicinity of the sliding surface $s \leq \sup |S_c \tilde{X}|$, and remaining within the sliding band.

Proof: Define the Lyapunov function as

$$V = \frac{1}{2} s^2 + \frac{1}{2\lambda_{ac}} (k_s - k_{s0})^2. \tag{21}$$

Substituting the expression for \dot{s} from (17), the derivative of V is obtained as

$$\begin{aligned} \dot{V} &= s \dot{s} + \frac{1}{\lambda_{ac}} (k_s - k_{s0}) (\dot{k}_s - \dot{k}_{s0}) \\ &= -s \left(S_c A \tilde{X} + S_c B \tilde{d} + k_s \text{sgn}(\hat{s}) \right) \\ &\quad + \frac{1}{\lambda_{ac}} (k_s - k_{s0}) (\dot{k}_s - \dot{k}_{s0}). \end{aligned} \tag{22}$$

We consider the condition that the system states are outside the sliding band, i.e., $s > \sup |S_c \tilde{X}|$. As noted in Remark 2, we now have $\text{sgn}(\hat{s}) = \text{sgn}(s + S_c \tilde{X}) = \text{sgn}(s)$. Then \dot{V} is rewritten as

$$\dot{V} = -s \left(S_c A \tilde{X} + S_c B \tilde{d} \right) - k_s |s| + \frac{1}{\lambda_{ac}} (k_s - k_{s0}) (\dot{k}_s - \dot{k}_{s0}). \tag{23}$$

The Lyapunov function is then discussed in the following two cases.

Case 1: if $k_s > k_{s0}$, according to the definition of k_{s0} from (19), we have

$$\begin{aligned}\dot{V}_1 &= -\left(S_c A \tilde{X} + S_c B \tilde{d}\right) s - k_s |s| \\ &< -\left(S_c A \tilde{X} + S_c B \tilde{d}\right) s - k_{s0} |s| \\ &< \left|S_c A \tilde{X} + S_c B \tilde{d}\right| |s| - k_{s0} |s| \\ &< 0.\end{aligned}$$

Furthermore, based on the definition of adaptive law (20) and the parameter tuning of λ_{ks} , we have

$$\begin{aligned}\dot{V}_2 &= \frac{1}{\lambda_{ac}} (k_s - k_{s0}) (\dot{k}_s - \dot{k}_{s0}) \\ &= \frac{1}{\lambda_{ac}} (k_s - k_{s0}) (-\lambda_{ks} - \lambda_{ac} (k_s - k_{s0}) - \dot{k}_{s0}) \\ &= -(k_s - k_{s0})^2 - \frac{1}{\lambda_{ac}} (k_s - k_{s0}) (\lambda_{ks} - \dot{k}_{s0}) \\ &< 0.\end{aligned}$$

Hence, in this case, $\dot{V} = \dot{V}_1 + \dot{V}_2 < 0$.

Case 2: if $k_s < k_{s0}$, by substituting definition of the adaptive law from (20), \dot{V} is further transformed into

$$\begin{aligned}\dot{V} &= -\left(S_c A \tilde{X} + S_c B \tilde{d}\right) s - k_{s0} |s| + (k_{s0} - k_s) |s| \\ &\quad + (k_s - k_{s0}) \left(\frac{\lambda_{ks} - \dot{k}_{s0}}{\lambda_{ac}} + k_{s0} - k_s + |\hat{s}|\right) \\ &= -\left(S_c A \tilde{X} + S_c B \tilde{d}\right) s - k_{s0} |s| \\ &\quad + (k_s - k_{s0}) \left(\frac{\lambda_{ks} - \dot{k}_{s0}}{\lambda_{ac}} - \left|S_c \tilde{X}\right|\right) - (k_{s0} - k_s)^2.\end{aligned}$$

Due to the parameter $\lambda_{ks} > \left|\dot{k}_{s0} + \lambda_{ac} \left|S_c \tilde{X}\right|\right|$, it follows that $\left(\frac{\lambda_{ks} - \dot{k}_{s0}}{\lambda_{ac}} - \left|S_c \tilde{X}\right|\right) > 0$. Therefore, in this case, we also have $\dot{V} < 0$.

Consequently, we can conclude that if the system states are outside the sliding band, the system will converge within the sliding boundaries that determined by the observation error under the proposed adaptive sliding mode control law. \square

IV. SIMULATION RESULTS

A. SIMULATION SETUP

This study employs the Amesim simulation platform to model and simulate the electro-hydraulic actuator for lifting loads. Amesim provides extensive libraries covering mechanical, power transmission, hydraulic components, and signal processing. These libraries support the development of a comprehensive simulation model for a practical EHA system, comprising the EHA itself, a pulley-wire rope lifting mechanism, a sliding mode controller, and observers, as depicted in Fig. 3. This model also accounts for additional components not explicitly addressed in the controller design, such as flushing valves, relief valves, pipelines, and the

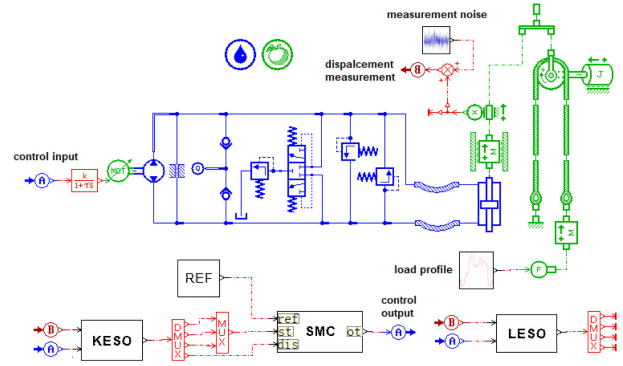


FIGURE 3. Simulation model of a practical EHA system in Amesim.

TABLE 1. Simulation parameters.

Parameters	Value	Units
A_p	7.854e-3	m
D_p	1.70e-5	m ³ /rad
m_p	1300	kg
β_e	900	MPa
C_t	4e-10	m ³ /s/Pa
V_c	0.5A _p	m ³
K_a	25.13	rad/s/V

electric motor. The parameters for the simulated system are listed in Table 1.

During the simulation, the EHA operates in a reciprocating motion to track a displacement trajectory with a trapezoidal velocity profile. The maximum stroke of the EHA is set to 1m, and the period of the motion cycle is 5s.

B. COMPARISON OF OBSERVERS

We compare the performance of LESO and KESO under two scenarios: noise-free measurements and measurements with noise. Both LESO and KESO receive the same displacement signal and control input to generate state observations and estimate the lumped disturbance. In this simulation, the sliding mode controller assumes knowledge of system states, using observers solely for state observation rather than closed-loop control.

1) MEASUREMENTS WITHOUT NOISE

The lumped disturbance's variance is calculated as $Q = 0.17$ based on the disturbance estimation results in Fig. 6. We assume zero variance for measurement noise in this case and assign a very small value of $R=1e-9$ for gain computation. The gain for KESO is computed as $K_1 = [38.356 \ 735.60 \ 325.10 \ 13115]^T$ using (10). In the case of LESO [28], the gain is designed by setting the equivalent bandwidth parameter ω_0 to 100, which exceeds the dynamics of the electro-hydraulic system. Consequently, the LESO gain is $L = [4\omega_0 \ 6\omega_0^2 \ 4\omega_0^3 \ \omega_0^4]^T$.

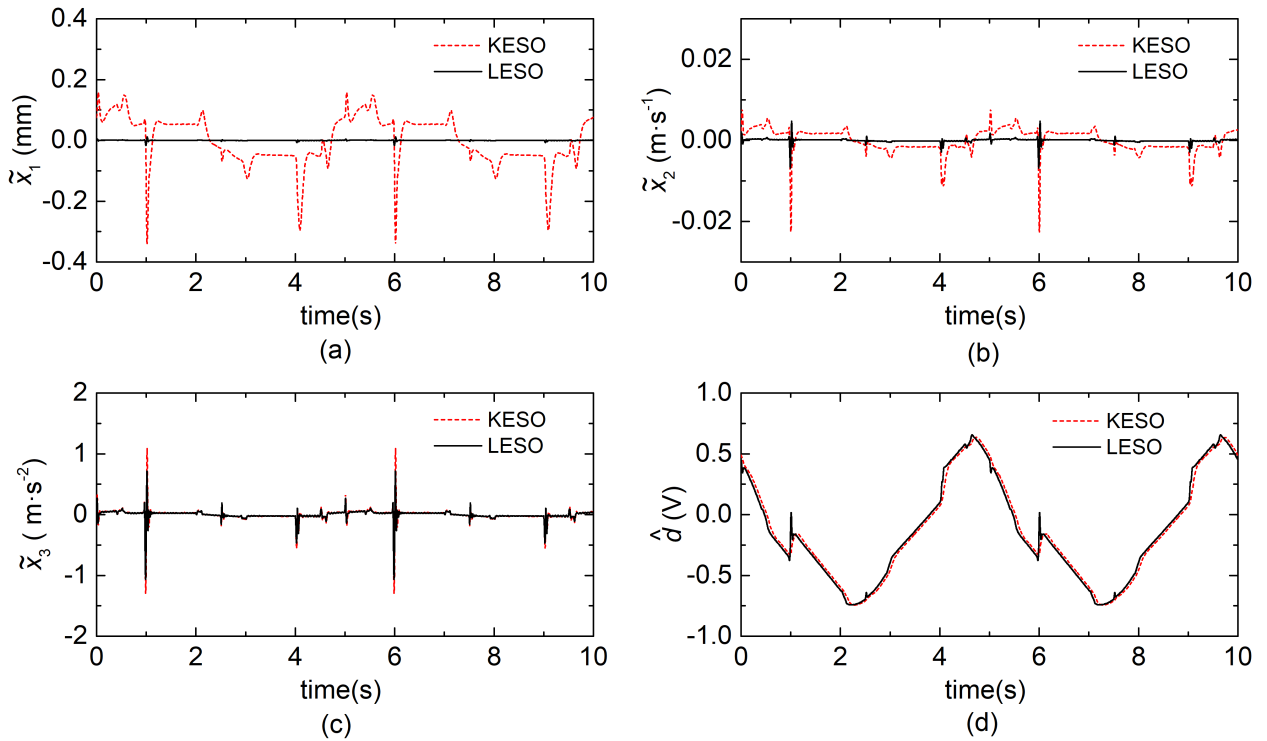


FIGURE 4. State observation errors and disturbance estimations without measurement noise: (a) Displacement observation errors, (b) Velocity observation errors, (c) Acceleration observation errors, (d) Estimated disturbances.

The state observation errors and disturbance estimations of the two observers in the condition of noise-free displacement measurements are presented in Fig. 4, while the mean and standard deviation of the absolute observation errors for the three states are listed in Table 2. It is evident that both KESO and LESO achieve satisfactory state observations in the absence of measurement noise, with the mean absolute error of x_1 less than 0.07mm. However, three key differences can be identified: (1) LESO, with its high-gain feedback, effectively suppresses unknown system disturbances, resulting in minimal displacement observation errors, whereas the low-gain KESO exhibits a maximum absolute displacement observation error of 0.36 mm. (2) Since only the displacement signal is available as the output, the advantage of high-gain feedback in LESO gradually diminishes in terms of velocity and acceleration observation accuracy, resulting in similar magnitudes of velocity and acceleration observation errors for both observers. (3) The disturbance estimation curves of both observers largely overlap, but due to KESO’s lower gain, its disturbance estimations display a slight time delay of 0.05s compared to LESO. Additionally, significant velocity and acceleration observation errors occur for both observers during the high-to-low pressure transition in fluid chambers of the EHA. This transition introduces model discontinuity and pressure impact, preventing the observers from accurately tracking abrupt changes in velocity and acceleration, resulting in notable errors.

2) MEASUREMENTS WITH NOISE

In this scenario, noise is introduced to the measurement signal. The noise includes white noise with a variance of $1e-7$, as well as small harmonic signals $1 \times 10^{-4} \sin(4\pi t)$ and $1 \times 10^{-5} \sin(40\pi t)$, as depicted in Fig. 5. The white noise arises from electromagnetic interference during the transmission of the measurement signal, and its variance is estimated based on actual usage patterns. The small harmonic noise is to mimic the low-frequency harmonic noise related to mechanical vibrations of the commonly used rope-type displacement sensors for long-stroke cylinders. The estimated variance of the process noise remains at 0.17. As a result, the gain of KESO in this condition is calculated as $K_2 = [11.977 \ 71.726 \ -3.0109 \ 1311.5]^T$.

Fig. 6 displays LESO’s observation results in the presence of measurement noise, where the high-gain LESO amplifies this noise, resulting in significantly noisy observations. The maximum absolute displacement error under the influence of noise is 0.5 mm, which may be considered acceptable. However, it is evident that the velocity and acceleration observations are significantly affected by severe noise contamination. Hence, the presented curves are the observations rather than errors. The estimated lumped disturbance is also heavily contaminated by noise. In this noisy measurement scenario, LESO loses its effectiveness. Consequently, we can conclude that while LESO exhibits satisfactory observation performance in the ideal noise-free conditions (Fig. 4), its

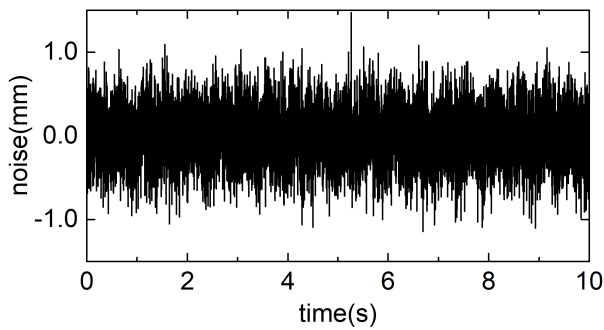


FIGURE 5. Measurement noise in the displacement output signal.

practical application in real systems with measurement noise may be constrained.

We also conduct a simulation experiment to assess the impact of adding a low-pass filter (LPF) before the LESO. A second-order LPF, featuring a fixed damping ratio of 0.707, is applied at the input of LESO. The cutoff frequency is determined based on the noise signal, with values set at $f_1 = 10\text{Hz}$ and $f_2 = 25\text{Hz}$. Fig. 7 illustrates the results of this “LPF + LESO” approach. In comparison to scenarios without the LPF, LESO’s observation performance is improved. However, an analysis of velocity, acceleration, and disturbance observations indicates that the LPF at both frequencies inadequately filters white noise in the measurement signal, resulting in significant spikes in the observed results. Moreover, opting for a lower LPF cutoff frequency f_1 yields a relatively higher noise reduction in the observation results compared to the higher cutoff frequency f_2 configuration. Nevertheless, the lower cutoff frequency f_1 introduces a larger phase lag, leading to greater displacement observation errors. In summary, the “LPF + LESO” approach fails to effectively suppress white noise in the measurement signal and introduces a significant phase lag, impacting the dynamic performance, as discussed in [40].

We further analysis the KESO under different feedback gains, providing an empirical guidance for tuning the parameters of KESO. Fig. 7 illustrates the observed results of the KESO under two gain conditions. K_1 and K_2 are computed above in the text, where K_1 represents a large gain associated with a low measurement-to-process noise variance ratio, and K_2 represents a small gain associated with a high measurement-to-process noise variance ratio. It can be noted that: (1) Employing a larger gain, K_1 , results in a smaller observation errors. The maximum absolute displacement observation error is 0.4 mm at K_1 , which is approximately one-third of the error at gain K_2 . This is due to the non-ideal white noise characteristics of the process noise, resulting in more significant suppression of process disturbance with a larger gain. (2) The error curve at K_1 , with a larger gain, shows more spikes compared to the curve at gain K_2 , indicating better suppression of random measurement white noise at gain K_2 . This aligns with the Kalman gain

calculation process, where large measurement noise leads to a smaller contribution of measured values to the estimated value compared to observed values. (3) The disturbance estimation at gain K_2 display smoother changes but with some phase lag.

Hence, while a small Kalman gain K_2 theoretically offers better accuracy under white noise conditions, opting for a larger Kalman gain proves more beneficial for effectively reducing non-white noise disturbances, improving state observation, and enhancing disturbance estimation. In practice, this feedback gain could be adjust according to the prior known statistic characteristics of the noise, and fine-tuning by trial-and-error. Table 2 lists the mean and standard deviation of state observation errors for the three observers, equally demonstrating that KESO with gain K_1 achieved the best observation performance.

C. EFFECTIVENESS OF THE ADAPTIVE SWITCHING-GAIN

In this subsection, we conducted a comparative analysis of the control performance of the sliding mode control law (15) using three sets of switching gains: $k_s = 200$, $k_s = 500$, and k_s automatically adjusted based on the adaptive law (20). It is assumed that the system state is known, measurement noise is neglected, and the observer is solely utilized for disturbance estimation. When employing the adaptive switching gain (20), the k_b within the desired switching-gain k_{s0} (19) is set to 200, while λ_{ks} and λ_{ac} are chosen as 100 and 30, respectively.

Fig. 8 illustrates the tracking errors of the EHA over two cycles with different switching-gain settings. The high-pressure and low-pressure chambers of the EHA undergo a switch at $t = 1.1\text{s}$ and 4.1s , resulting in a peak tracking error of 0.89 mm during this disturbance process when $k_s = 200$. These observations indicate that the switching gain k_s is not sufficiently large to suppress the disturbance effectively during these instances. The system’s tracking error consistently decreases throughout the entire duration when $k_s = 500$, with a notable reduction during pressure switching, resulting in a maximum tracking error decrease to 0.12 mm. By employing adaptive switching gain, the tracking error remains nearly identical to $k_s = 500$, while further reducing the maximum tracking error to 0.04 mm during pressure switching.

Fig. 9 depicts the switching gain employed during its adaptation, which adjusts in response to disturbance changes and varies above the base switching gain k_b . At $t = 1.1\text{s}$, the adaptive switching gain reaches its peak value of 749 and then decreases rapidly. This suggests that using a fixed switching gain of 500 is insufficient at this specific moment, leading to reduced tracking errors when using adaptive gain, as shown in Fig. 8. Hence, this demonstrates the capability of the proposed adaptation law to detect changes in the sliding variable induced by disturbances and automatically adjust the switching gain to match the desired value.

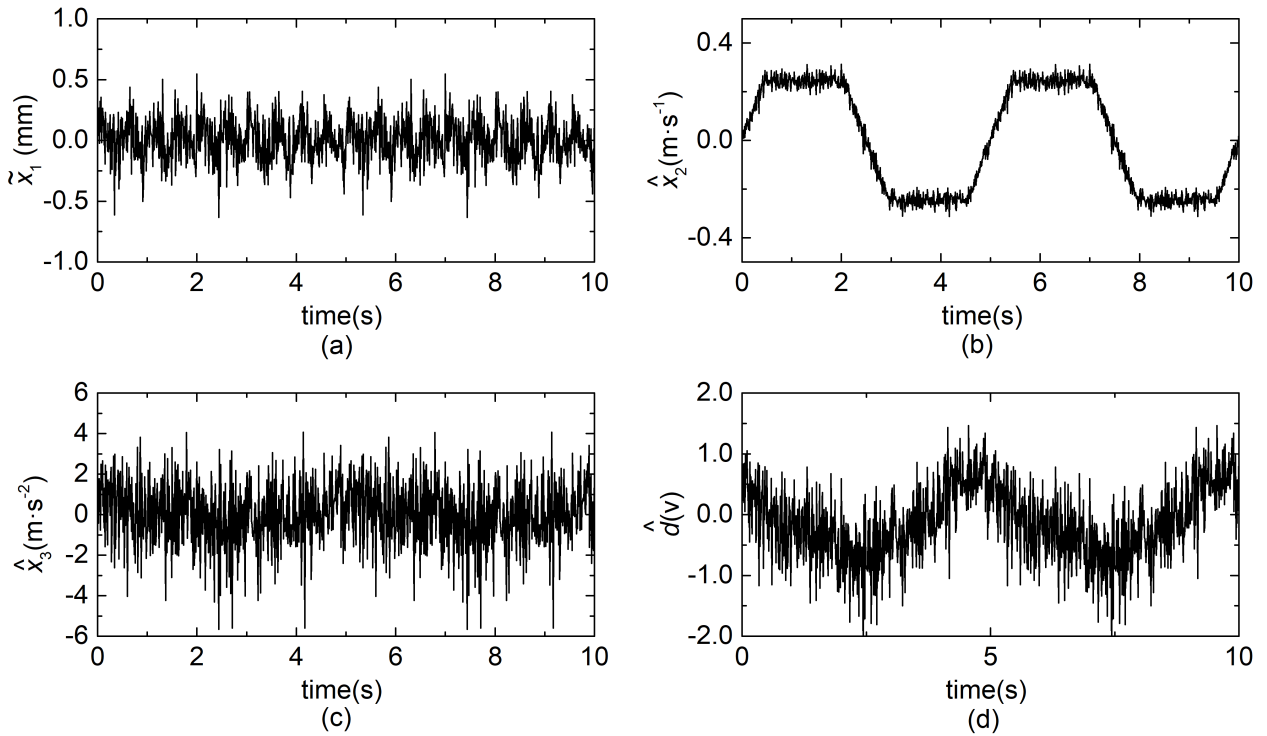


FIGURE 6. Observation results of LESO in the presence of measurement noise: (a) Displacement observation errors, (b) Observed velocity values, (c) Observed acceleration values, (d) Estimated disturbances.

TABLE 2. Comparison of observation errors between KESO and LESO.

		$ \tilde{x}_1 $		$ \tilde{x}_2 $		$ \tilde{x}_3 $	
		mean	std	mean	std	mean	std
without	KESO	0.0659	0.0448	0.0022	0.0020	0.0524	0.1208
meas. noise	LESO	0.0007	0.0014	0.0003	0.0006	0.0440	0.0978
with	KESO (K_1)	0.0917	0.0607	0.0020	0.0019	0.0527	0.1195
	KESO (K_2)	0.4295	0.2325	0.0055	0.0031	0.0520	0.1196
	LESO	0.1459	0.1075	0.0187	0.0142	1.1980	0.9396

D. POSITION TRACKING WITH KESO FOR STATE OBSERVATION

1) COMPARISON WITH KNOWN STATE CONDITION

Now we investigated the EHA tracking control problem with noisy displacement measurements by combining ASMC with KESO. In Fig. 10, two curves depict the displacement observation error $\tilde{x}_1 = \hat{x}_1 - x_1$ and the displacement tracking error $e_1 = x_1 - x_d$, showing approximate symmetry around the x-axis. This behavior is due to the sliding mode controller, which ensures that \hat{x}_1 approximates x_d after processing the state observation, as opposed to x_1 approaching x_d in a known state condition. Therefore, the tracking error $e_1 \approx x_1 - \hat{x}_1 = -\tilde{x}_1$ can be obtained, as shown by the two curves in Fig. 10. The maximum absolute value of e_1 is 1.03 mm, slightly exceeding the 0.77 mm amplitude of the \tilde{x}_1 , and significantly greater than the 0.04 mm amplitude in the known state condition. This result suggests that introducing a state observer will primarily include state observation error

in the tracking error, further compounded by the control-induced tracking error, resulting in a slightly higher final tracking error compared to the observation error. In contrast, in the known state condition, the tracking error is minimized.

The estimated and true values of the sliding variable are presented in Fig. 11. While the estimated value \hat{s} remains close to zero, the true value s fluctuates around the x-axis. This demonstrates that using sliding mode control with a state observer confines the observed state to the sliding surface instead of the true state. Furthermore, state-observed sliding mode control naturally introduces a boundary layer whose thickness correlates with the state observation error, as explained in Remark 2.

Fig. 12 illustrates the adaptive switching gain, which varies with system disturbances. In the presence of significant tracking errors caused by disturbances, the switching gain rapidly increases, keeping the tracking error only slightly larger than the state observation error. Compared to the

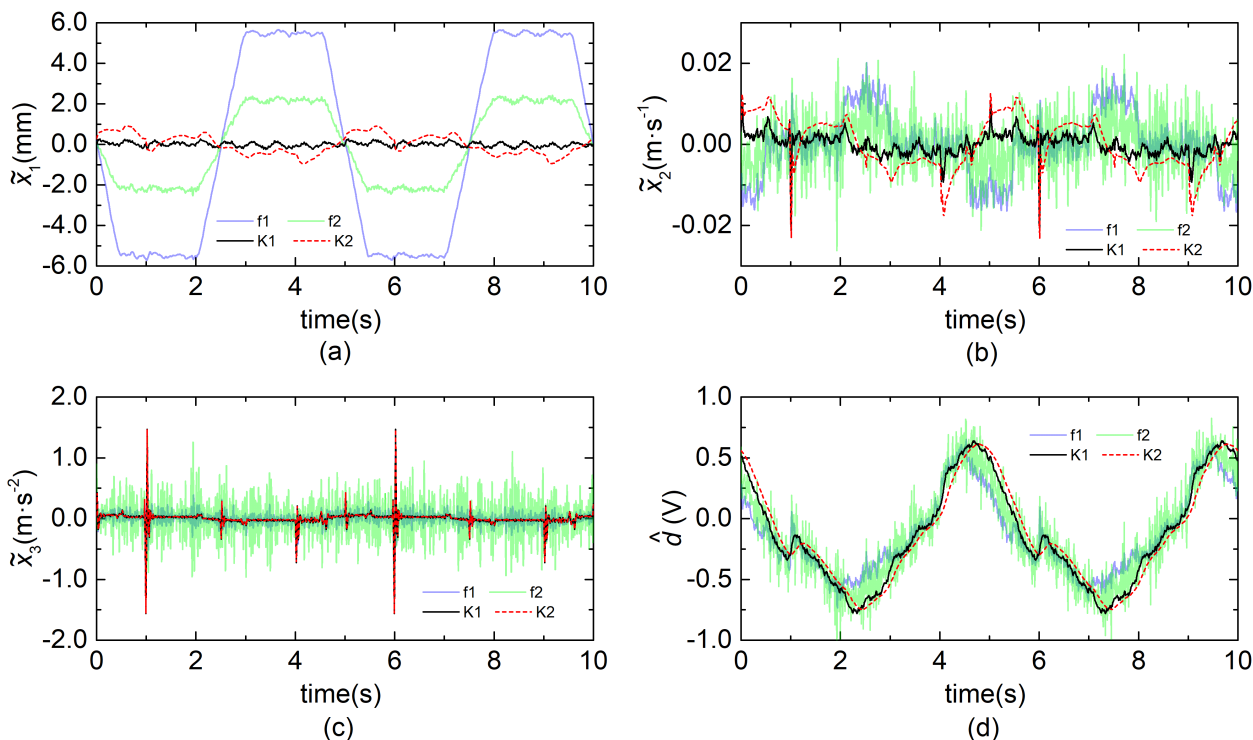


FIGURE 7. Observation results of the “LPF + LESO” method (with cutoff frequencies f_1 and f_2) and the KESO (with gains K_1 and K_2) in the presence of measurement noise: (a) Displacement observation errors, (b) Velocity observation errors, (c) Acceleration observation errors, (d) Estimated disturbances.

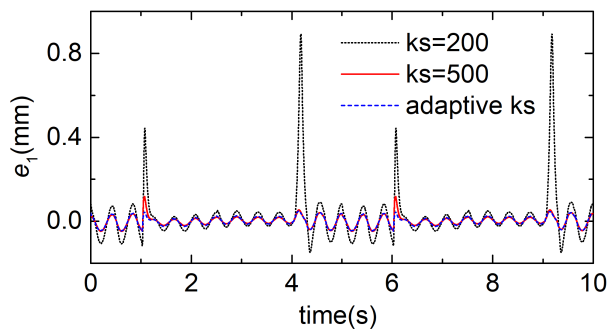


FIGURE 8. Tracking errors of the EHA under different switching-gain conditions without measurement noise.

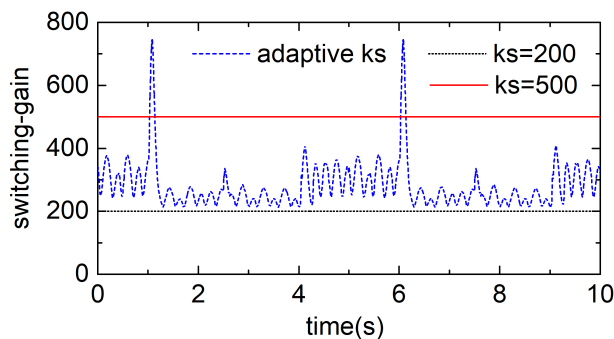


FIGURE 9. Switching-gain adaptation without measurement noise.

maximum adaptive switching gain of 749 in the known state condition, the maximum adaptive switching gain under state observation conditions is reduced significantly to 404. This reduction is credited to KESO’s filtering effect, which lowers the changing rate in the sliding variable and the switching action, leading to a decreased calculation of the desired switching gain.

Hence, during EHA displacement tracking with KESO-ASMC, the observer configuration significantly influences tracking performance, and the displacement tracking error is mainly determined by the displacement observation error. When employing larger Kalman gains, KESO effectively suppresses non-white random disturbances, thereby reducing observation errors. However, this may weaken filtering

effect on white noise in the measurement, leading to signal processing failure. Conversely, smaller Kalman gains provide good white noise filtering capabilities but poorly suppress random disturbances, resulting in larger observation errors. Therefore, fine-tuning the Kalman gains of KESO is necessary through an iterative approach to strike a balance between observation errors and observation noise suppression, ultimately achieving optimal displacement tracking performance.

2) COMPARISON WITH THE PID CONTROLLER

We assess the control performance of KESO-ASMC against the widely used PID controller, which dominates industrial applications and serves as a practical baseline for control

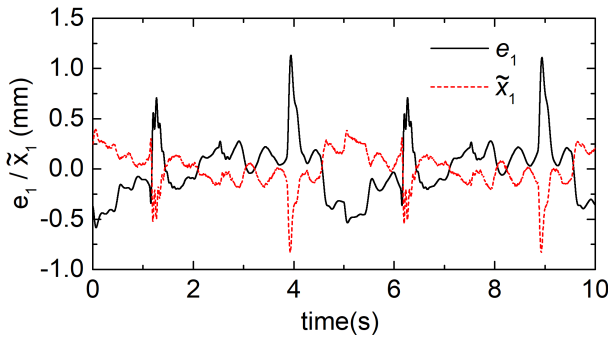


FIGURE 10. Displacement tracking error e_1 and observation error \tilde{x}_1 in KESO-ASMC.

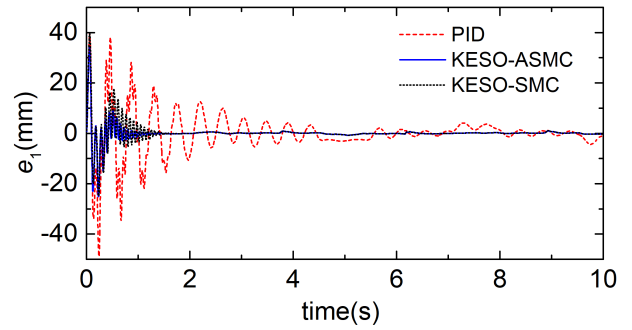


FIGURE 13. Displacement tracking errors from simulation start for three controllers.

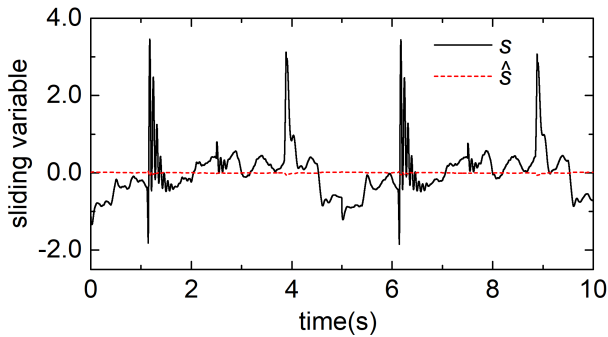


FIGURE 11. Estimated and true values of the sliding variable.

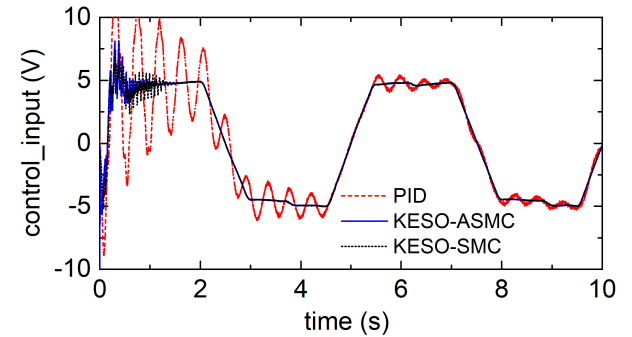


FIGURE 14. Control actions from simulation start for three controllers.

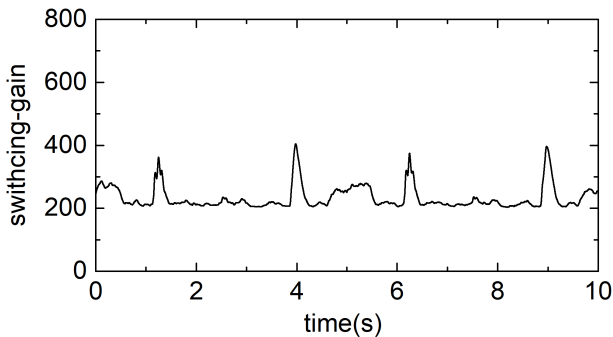


FIGURE 12. Adaptive switching gain in the observed state condition.

TABLE 3. Comparison of tracking errors among three controllers.

	MAAE	MAE	IAE
PID	50.40	4.66	46.64
KESO-ASMC	35.00	0.83	8.27
KESO-SMC	40.50	1.13	11.29

performance. In this subsection, we focus on the first two simulation cycles, which differs from prior comparisons that concerning the last two cycles of the simulation. The PID controller is initially configured using the Ziegler-Nichols closed-loop tuning method to find the initial parameters, and then its parameter is further tuned by trial-and-error through

batch simulations. Finally, the PID controller attains nearly optimal parameters: $k_p = 62$, $k_i = 3900$, $k_d = 0.61$.

Fig. 13 depicts the performance of three controllers: the PID controller, the proposed KESO-ASMC, and KESO-SMC (sliding mode control with a constant gain of 500) in tracking the displacement of the EHA. Tracking errors for these controllers are illustrated across two motion cycles, commencing from the simulation’s initiation. Because of notable disparities in system state values between the initial simulation phase and normal runtime, it’s like introducing an initial disturbance in the early simulation stage, leading to significant tracking errors for all three controllers during this phase. In comparison to the sliding mode controller, the PID controller exhibits more pronounced error oscillations in terms of both magnitude and duration. Conversely, KESO-ASMC adjust its switching to the maximum permitted value (set to 8000 in the simulation) in face of the large disturbance at the beginning of the simulation, and rapidly converges to a stable tracking error through a dynamic switching gain approach. Additionally, control performance is evaluated using metrics such as Maximum Absolute Error (MAAE), Mean Absolute Error (MAE), and Integral Absolute Error (IAE). A summary of these performance indices is presented in Table 3. It is evident that KESO-ASMC outperforms the other two controllers across all three metrics, showcasing its capability to effectively mitigate disturbances, even in the presence of measurement noise, and ensure high-precision tracking control.

Another drawback of the PID controller, in comparison to KESO-ASMC, is the relatively high noise in the control action. Adaptive sliding mode control with KESO effectively suppresses white noise in the measurement signal, while the high-gain feedback in PID control amplifies it, as shown in Fig. 14. Therefore, the KESO-ASMC method proposed in this paper is more practical than the traditional PID controller in noisy measurement conditions.

V. CONCLUSION

This paper presents an adaptive sliding mode control scheme that integrates the Kalman extended state observer for tracking control of electro-hydraulic actuators in the presence of noisy displacement measurements. By utilizing the Kalman filtering technique to tune the observer gain of the LESO, simultaneous state observation and disturbance estimation are effectively achieved in the presence of measurement noise. To ensure control performance and reduce chattering, the proposed adaptive switching gain method, which is based on its desired value, tracks disturbance variations and dynamically adjusts the gain to keep it slightly larger than the required value. Simulation results demonstrate that the proposed control scheme is capable of real-world control of EHAs with measurement noise and unknown disturbances. The proposed method is conceptually simple and straightforward to implement, yet it still requires some prior knowledge and parameter tuning. In future work, methods such as neural adaptive techniques will be explored further to address these constraints.

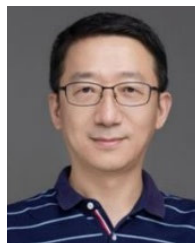
REFERENCES

- [1] H. Liu, X. Zhang, L. Quan, and H. Zhang, "Research on energy consumption of injection molding machine driven by five different types of electro-hydraulic power units," *J. Cleaner Prod.*, vol. 242, Jan. 2020, Art. no. 118355, doi: [10.1016/j.jclepro.2019.118355](https://doi.org/10.1016/j.jclepro.2019.118355).
- [2] L. Wang, X. Yang, G. Gong, and J. Du, "Pose and trajectory control of shield tunneling machine in complicated stratum," *Autom. Construct.*, vol. 93, pp. 192–199, Sep. 2018, doi: [10.1016/j.autcon.2018.05.020](https://doi.org/10.1016/j.autcon.2018.05.020).
- [3] S. Zhao, K. Chen, X. Zhang, Y. Zhao, G. Jing, C. Yin, and X. Xiao, "A high-order load model and the control algorithm for an aerospace electro-hydraulic actuator," *Actuators*, vol. 10, no. 3, p. 53, Mar. 2021, doi: [10.3390/act10030053](https://doi.org/10.3390/act10030053).
- [4] S. A. Ali, A. Christen, S. Begg, and N. Langlois, "Continuous–discrete time-observer design for state and disturbance estimation of electro-hydraulic actuator systems," *IEEE Trans. Ind. Electron.*, vol. 63, no. 7, pp. 4314–4324, Jul. 2016, doi: [10.1109/TIE.2016.2531022](https://doi.org/10.1109/TIE.2016.2531022).
- [5] V. D. Phan, H. V. A. Truong, and K. K. Ahn, "Actuator failure compensation-based command filtered control of electro-hydraulic system with position constraint," *ISA Trans.*, vol. 134, pp. 561–572, Mar. 2023, doi: [10.1016/j.isatra.2022.08.023](https://doi.org/10.1016/j.isatra.2022.08.023).
- [6] W. Shen, S. Liu, and M. Liu, "Adaptive sliding mode control of hydraulic systems with the event trigger and finite-time disturbance observer," *Inf. Sci.*, vol. 569, pp. 55–69, Aug. 2021, doi: [10.1016/j.ins.2021.03.051](https://doi.org/10.1016/j.ins.2021.03.051).
- [7] Z. Yao, X. Liang, Q. Zhao, and J. Yao, "Adaptive disturbance observer-based control of hydraulic systems with asymptotic stability," *Appl. Math. Model.*, vol. 105, pp. 226–242, May 2022, doi: [10.1016/j.apm.2021.12.026](https://doi.org/10.1016/j.apm.2021.12.026).
- [8] G. Palli, S. Strano, and M. Terzo, "Sliding-mode observers for state and disturbance estimation in electro-hydraulic systems," *Control Eng. Pract.*, vol. 74, pp. 58–70, May 2018, doi: [10.1016/j.conengprac.2018.02.007](https://doi.org/10.1016/j.conengprac.2018.02.007).
- [9] L. Wang, D. Zhao, Z. Zhang, Q. Liu, F. Liu, and T. Jia, "Model-free linear active disturbance rejection output feedback control for electro-hydraulic proportional system with unknown dead-zone," *IET Control Theory Appl.*, vol. 15, no. 16, pp. 2081–2094, Aug. 2021, doi: [10.1049/cth2.12177](https://doi.org/10.1049/cth2.12177).
- [10] M. H. Nguyen, H. V. Dao, and K. K. Ahn, "Active disturbance rejection control for position tracking of electro-hydraulic servo systems under modeling uncertainty and external load," *Actuators*, vol. 10, no. 2, p. 20, Jan. 2021, doi: [10.3390/act10020020](https://doi.org/10.3390/act10020020).
- [11] Z. Has, M. F. Rahmat, A. R. Husain, and M. N. Ahmad, "Robust precision control for a class of electro-hydraulic actuator system based on disturbance observer," *Int. J. Precis. Eng. Manuf.*, vol. 16, no. 8, pp. 1753–1760, Jul. 2015, doi: [10.1007/s12541-015-0230-y](https://doi.org/10.1007/s12541-015-0230-y).
- [12] M. Fallahi, M. Zareinejad, K. Baghestan, A. Tivay, S. M. Rezaei, and A. Abdullah, "Precise position control of an electro-hydraulic servo system via robust linear approximation," *ISA Trans.*, vol. 80, pp. 503–512, Sep. 2018, doi: [10.1016/j.isatra.2018.06.002](https://doi.org/10.1016/j.isatra.2018.06.002).
- [13] S. Liu, R. Hao, D. Zhao, and Z. Tian, "Adaptive dynamic surface control for active suspension with electro-hydraulic actuator parameter uncertainty and external disturbance," *IEEE Access*, vol. 8, pp. 156645–156653, 2020, doi: [10.1109/ACCESS.2020.3018442](https://doi.org/10.1109/ACCESS.2020.3018442).
- [14] S. Li, J. Yang, W.-H. Chen, and X. Chen, *Disturbance Observer-Based Control*. Boca Raton, FL, USA: CRC Press, 2014, doi: [10.1201/b16570](https://doi.org/10.1201/b16570).
- [15] Q. Zou, "Extended state observer-based finite time control of electro-hydraulic system via sliding mode technique," *Asian J. Control*, vol. 24, no. 5, pp. 2311–2327, Aug. 2021, doi: [10.1002/asjc.2638](https://doi.org/10.1002/asjc.2638).
- [16] W. Deng and J. Yao, "Extended-state-observer-based adaptive control of electrohydraulic servomechanisms without velocity measurement," *IEEE/ASME Trans. Mechatronics*, vol. 25, no. 3, pp. 1151–1161, Jun. 2020, doi: [10.1109/TMECH.2019.2959297](https://doi.org/10.1109/TMECH.2019.2959297).
- [17] W.-H. Chen, J. Yang, L. Guo, and S. Li, "Disturbance-observer-based control and related methods—An overview," *IEEE Trans. Ind. Electron.*, vol. 63, no. 2, pp. 1083–1095, Feb. 2016, doi: [10.1109/TIE.2015.2478397](https://doi.org/10.1109/TIE.2015.2478397).
- [18] H. Ho Choi, "Sliding-mode output feedback control design," *IEEE Trans. Ind. Electron.*, vol. 55, no. 11, pp. 4047–4054, Nov. 2008, doi: [10.1109/TIE.2008.2004386](https://doi.org/10.1109/TIE.2008.2004386).
- [19] W.-H. Chen, D. J. Ballance, P. J. Gawthrop, and J. O'Reilly, "A nonlinear disturbance observer for robotic manipulators," *IEEE Trans. Ind. Electron.*, vol. 47, no. 4, pp. 932–938, 2000, doi: [10.1109/41.857974](https://doi.org/10.1109/41.857974).
- [20] V. D. Phan and K. K. Ahn, "Optimized-based fault-tolerant control of an electro-hydraulic system with disturbance rejection," *Appl. Sci.*, vol. 12, no. 18, p. 9197, Sep. 2022, doi: [10.3390/app12189197](https://doi.org/10.3390/app12189197).
- [21] D. X. Ba, T. Q. Dinh, J. Bae, and K. K. Ahn, "An effective disturbance-observer-based nonlinear controller for a pump-controlled hydraulic system," *IEEE/ASME Trans. Mechatronics*, vol. 25, no. 1, pp. 32–43, Feb. 2020, doi: [10.1109/TMECH.2019.2946871](https://doi.org/10.1109/TMECH.2019.2946871).
- [22] N. Sacchi, G. P. Incremona, and A. Ferrara, "Neural network-based practical/ideal integral sliding mode control," *IEEE Control Syst. Lett.*, vol. 6, pp. 3140–3145, 2022, doi: [10.1109/LCSYS.2022.3182814](https://doi.org/10.1109/LCSYS.2022.3182814).
- [23] T. Zou, H. Wu, W. Sun, and Z. Zhao, "Adaptive neural network sliding mode control of a nonlinear two-degrees-of-freedom helicopter system," *Asian J. Control*, vol. 25, no. 3, pp. 2085–2094, May 2023, doi: [10.1002/asjc.2862](https://doi.org/10.1002/asjc.2862).
- [24] T. N. Truong, A. T. Vo, and H.-J. Kang, "An adaptive terminal sliding mode control scheme via neural network approach for path-following control of uncertain nonlinear systems," *Int. J. Control, Autom. Syst.*, vol. 20, no. 6, pp. 2081–2096, Jun. 2022, doi: [10.1007/s12555-021-0239-1](https://doi.org/10.1007/s12555-021-0239-1).
- [25] J. Fei, Z. Wang, X. Liang, Z. Feng, and Y. Xue, "Fractional sliding-mode control for microgyroscope based on multilayer recurrent fuzzy neural network," *IEEE Trans. Fuzzy Syst.*, vol. 30, no. 6, pp. 1712–1721, Jun. 2022, doi: [10.1109/TFUZZ.2021.3064704](https://doi.org/10.1109/TFUZZ.2021.3064704).
- [26] T. N. Truong, A. T. Vo, and H.-J. Kang, "Implementation of an adaptive neural terminal sliding mode for tracking control of magnetic levitation systems," *IEEE Access*, vol. 8, pp. 206931–206941, 2020, doi: [10.1109/ACCESS.2020.3036010](https://doi.org/10.1109/ACCESS.2020.3036010).
- [27] J. Han, "From PID to active disturbance rejection control," *IEEE Trans. Ind. Electron.*, vol. 56, no. 3, pp. 900–906, Mar. 2009, doi: [10.1109/TIE.2008.2011621](https://doi.org/10.1109/TIE.2008.2011621).
- [28] Q. Zheng, L. Q. Gaol, and Z. Gao, "On stability analysis of active disturbance rejection control for nonlinear time-varying plants with unknown dynamics," in *Proc. 46th IEEE Conf. Decis. Control*, Dec. 2007, pp. 3501–3506, doi: [10.1109/CDC.2007.4434676](https://doi.org/10.1109/CDC.2007.4434676).
- [29] D. Yoo, S. S.-T. Yau, and Z. Gao, "Optimal fast tracking observer bandwidth of the linear extended state observer," *Int. J. Control*, vol. 80, no. 1, pp. 102–111, Jan. 2007, doi: [10.1080/00207170600936555](https://doi.org/10.1080/00207170600936555).
- [30] S. A. Khan, Y. Guo, Y. P. Siwakoti, D. D. Lu, and J. Zhu, "A disturbance rejection-based control strategy for five-level T-type hybrid power converters with ripple voltage estimation capability," *IEEE Trans. Ind. Electron.*, vol. 67, no. 9, pp. 7364–7374, Sep. 2020, doi: [10.1109/TIE.2019.2942550](https://doi.org/10.1109/TIE.2019.2942550).

- [31] J. Liu, S. Vazquez, L. Wu, A. Marquez, H. Gao, and L. G. Franquelo, "Extended state observer-based sliding-mode control for three-phase power converters," *IEEE Trans. Ind. Electron.*, vol. 64, no. 1, pp. 22–31, Jan. 2017, doi: [10.1109/TIE.2016.2610400](https://doi.org/10.1109/TIE.2016.2610400).
- [32] K. Rsetam, Z. Cao, and Z. Man, "Cascaded-extended-state-observer-based sliding-mode control for underactuated flexible joint robot," *IEEE Trans. Ind. Electron.*, vol. 67, no. 12, pp. 10822–10832, Dec. 2020, doi: [10.1109/TIE.2019.2958283](https://doi.org/10.1109/TIE.2019.2958283).
- [33] Z. Xu, X. Yang, S. Zhou, W. Zhang, W. Zhang, S. Yang, and P. X. Liu, "Extended state observer based adaptive backstepping nonsingular fast terminal sliding-mode control for robotic manipulators with uncertainties," *Int. J. Control. Autom. Syst.*, vol. 20, no. 9, pp. 2972–2982, Sep. 2022, doi: [10.1007/s12555-021-0559-1](https://doi.org/10.1007/s12555-021-0559-1).
- [34] H. Wang, N. Li, Y. Wang, and B. Su, "Backstepping sliding mode trajectory tracking via extended state observer for quadrotors with wind disturbance," *Int. J. Control. Autom. Syst.*, vol. 19, no. 10, pp. 3273–3284, Oct. 2021, doi: [10.1007/s12555-020-0673-5](https://doi.org/10.1007/s12555-020-0673-5).
- [35] J. Xiong, J. Pan, G. Chen, X. Zhang, and F. Ding, "Sliding mode dual-channel disturbance rejection attitude control for a quadrotor," *IEEE Trans. Ind. Electron.*, vol. 69, no. 10, pp. 10489–10499, Oct. 2022, doi: [10.1109/TIE.2021.3137600](https://doi.org/10.1109/TIE.2021.3137600).
- [36] J. Yao, Z. Jiao, and D. Ma, "Extended-state-observer-based output feedback nonlinear robust control of hydraulic systems with backstepping," *IEEE Trans. Ind. Electron.*, vol. 61, no. 11, pp. 6285–6293, Nov. 2014, doi: [10.1109/TIE.2014.2304912](https://doi.org/10.1109/TIE.2014.2304912).
- [37] Z. Xu, W. Deng, H. Shen, and J. Yao, "Extended-state-observer-based adaptive prescribed performance control for hydraulic systems with full-state constraints," *IEEE/ASME Trans. Mechatronics*, vol. 27, no. 6, pp. 5615–5625, Dec. 2022, doi: [10.1109/TMECH.2022.3186390](https://doi.org/10.1109/TMECH.2022.3186390).
- [38] C. Wang, Z. Zhang, H. Wang, B. Zhao, and L. Quan, "Disturbance observer-based output feedback control of hydraulic servo system considering mismatched uncertainties and internal pressure dynamics stability," *IET Control Theory Appl.*, vol. 14, no. 8, pp. 1046–1056, May 2020, doi: [10.1049/iet-cta.2019.0346](https://doi.org/10.1049/iet-cta.2019.0346).
- [39] Z. Zhang, Y. Guo, D. Gong, and J. Liu, "Global integral sliding-mode control with improved nonlinear extended state observer for rotary tracking of a hydraulic roofbolter," *IEEE/ASME Trans. Mechatronics*, vol. 28, no. 1, pp. 483–494, Feb. 2023, doi: [10.1109/TMECH.2022.3203517](https://doi.org/10.1109/TMECH.2022.3203517).
- [40] O. Babayomi and Z. Zhang, "Model-free predictive control of power converters with cascade-parallel extended state observers," *IEEE Trans. Ind. Electron.*, vol. 70, no. 10, pp. 10215–10226, Oct. 2023, doi: [10.1109/TIE.2022.3217609](https://doi.org/10.1109/TIE.2022.3217609).
- [41] Z. Xu, X. Yang, W. Zhang, W. Zhang, L. Zhang, and P. X. Liu, "Backstepping sliding mode control based on extended state observer for robotic manipulators with LuGre friction," *Int. J. Control. Autom. Syst.*, vol. 20, no. 6, pp. 2054–2066, Jun. 2022, doi: [10.1007/s12555-020-0738-5](https://doi.org/10.1007/s12555-020-0738-5).
- [42] L. Chen, Z. Liu, Q. Dang, W. Zhao, and G. Wang, "Robust trajectory tracking control for a quadrotor using recursive sliding mode control and nonlinear extended state observer," *Aerosp. Sci. Technol.*, vol. 128, Sep. 2022, Art. no. 107749, doi: [10.1016/j.ast.2022.107749](https://doi.org/10.1016/j.ast.2022.107749).
- [43] C. Ren, X. Li, X. Yang, and S. Ma, "Extended state observer-based sliding mode control of an omnidirectional mobile robot with friction compensation," *IEEE Trans. Ind. Electron.*, vol. 66, no. 12, pp. 9480–9489, Dec. 2019, doi: [10.1109/TIE.2019.2892678](https://doi.org/10.1109/TIE.2019.2892678).
- [44] X. Yuan, Y. Zuo, Y. Fan, and C. H. T. Lee, "Model-free predictive current control of SPMSM drives using extended state observer," *IEEE Trans. Ind. Electron.*, vol. 69, no. 7, pp. 6540–6550, Jul. 2022, doi: [10.1109/TIE.2021.3095816](https://doi.org/10.1109/TIE.2021.3095816).
- [45] Z. Zhang, Y. Guo, D. Gong, and S. Zhu, "Improved extended state observer-based global sliding-mode finite-time control for displacement tracking of a hydraulic roofbolter," *Nonlinear Dyn.*, vol. 111, no. 12, pp. 11191–11203, Jun. 2023, doi: [10.1007/s11071-023-08440-8](https://doi.org/10.1007/s11071-023-08440-8).
- [46] B. L. Cong, Z. Chen, and X. D. Liu, "On adaptive sliding mode control without switching gain overestimation," *Int. J. Robust Nonlinear Control*, vol. 24, no. 3, pp. 515–531, Sep. 2012, doi: [10.1002/rnc.2902](https://doi.org/10.1002/rnc.2902).
- [47] O. Barambones and P. Alkorta, "Position control of the induction motor using an adaptive sliding-mode controller and observers," *IEEE Trans. Ind. Electron.*, vol. 61, no. 12, pp. 6556–6565, Dec. 2014, doi: [10.1109/TIE.2014.2316239](https://doi.org/10.1109/TIE.2014.2316239).
- [48] D. Tian, R. Xu, E. Sariyildiz, and H. Gao, "An adaptive switching-gain sliding-mode-assisted disturbance observer for high-precision servo control," *IEEE Trans. Ind. Electron.*, vol. 69, no. 2, pp. 1762–1772, Feb. 2022, doi: [10.1109/TIE.2021.3057004](https://doi.org/10.1109/TIE.2021.3057004).
- [49] P. Li, X. Yu, and Y. Zhang, "The design of quasi-optimal higher order sliding mode control via disturbance observer and switching-gain adaptation," *IEEE Trans. Syst., Man, Cybern., Syst.*, vol. 50, no. 11, pp. 4817–4827, Nov. 2020, doi: [10.1109/TSMC.2018.2866856](https://doi.org/10.1109/TSMC.2018.2866856).
- [50] D. T. Tran, D. X. Ba, and K. K. Ahn, "Adaptive backstepping sliding mode control for equilibrium position tracking of an electrohydraulic elastic manipulator," *IEEE Trans. Ind. Electron.*, vol. 67, no. 5, pp. 3860–3869, May 2020, doi: [10.1109/TIE.2019.2918475](https://doi.org/10.1109/TIE.2019.2918475).
- [51] S. Baek, J. Baek, and S. Han, "An adaptive sliding mode control with effective switching gain tuning near the sliding surface," *IEEE Access*, vol. 7, pp. 15563–15572, 2019, doi: [10.1109/ACCESS.2019.2894911](https://doi.org/10.1109/ACCESS.2019.2894911).
- [52] C. Wang, H. Xia, Y. Wang, and S. Ren, "A novel adaptive-gain higher-order sliding mode controller and its parameters tuning," *Nonlinear Dyn.*, vol. 107, no. 1, pp. 1049–1062, Nov. 2021, doi: [10.1007/s11071-021-07037-3](https://doi.org/10.1007/s11071-021-07037-3).
- [53] F. Auger, M. Hilairet, J. M. Guerrero, E. Monmasson, T. Orłowska-Kowalska, and S. Katsura, "Industrial applications of the Kalman filter: A review," *IEEE Trans. Ind. Electron.*, vol. 60, no. 12, pp. 5458–5471, Dec. 2013, doi: [10.1109/TIE.2012.2236994](https://doi.org/10.1109/TIE.2012.2236994).
- [54] B. Ni and Q. Zhang, "Stability of the Kalman filter for continuous time output error systems," *Syst. Control Lett.*, vol. 94, pp. 172–180, Aug. 2016, doi: [10.1016/j.sysconle.2016.06.006](https://doi.org/10.1016/j.sysconle.2016.06.006).
- [55] H. Yang, L. Cheng, J. Zhang, and Y. Xia, "Leader-follower trajectory control for quadrotors via tracking differentiators and disturbance observers," *IEEE Trans. Syst., Man, Cybern., Syst.*, vol. 51, no. 1, pp. 601–609, Jan. 2021, doi: [10.1109/TSMC.2018.2872872](https://doi.org/10.1109/TSMC.2018.2872872).
- [56] H. Zhou, L. Lao, Y. Chen, and H. Yang, "Discrete-time sliding mode control with an input filter for an electro-hydraulic actuator," *IET Control Theory Appl.*, vol. 11, no. 9, pp. 1333–1340, Jun. 2017, doi: [10.1049/iet-cta.2016.0951](https://doi.org/10.1049/iet-cta.2016.0951).



LIMING LAO received the B.S. and Ph.D. degrees in mechatronics engineering from Zhejiang University, Hangzhou, China, in 2010 and 2017, respectively. He is currently a Lecturer with the Institute of Robotics and Intelligent Systems, Taizhou University, Taizhou, Zhejiang, China. His research interests include robotics, the servo control of mechatronic systems, and human-robot interactions.



PENGZHAN CHEN received the B.S. and M.S. degrees from the School of Aeronautical Manufacturing Engineering, Nanchang Hangkong University, Nanchang, Jiangxi, China, in 1997 and 2000, respectively, and the Ph.D. degree from the School of Mechanical Science and Engineering, Huazhong University of Science and Technology, Wuhan, Hubei, China, in 2010. He is currently a Professor with the School of Intelligent Manufacturing, Taizhou University, Taizhou, Zhejiang, China. His current research interests include intelligent robot systems and human-robot cooperation.

• • •